Neural Network Model for Isothermal Pearlite Transformation.

Part II: Growth Rate Model

C. CAPDEVILA, F. G. CABALLERO, and C. GARCÍA DE ANDRÉS

Dr. C. Capdevila and Dr. F. G. Caballero, Tenured Scientist, and Dr. C. García de Andrés, Research Scientist, are in the Department of Physical Metallurgy, Centro Nacional de Investigaciones Metalúrgicas (CENIM), CSIC, Avda. Gregorio del Amo, 8, 28040 Madrid, Spain..

Abstract

The pearlite growth rate during the isothermal austenite-to-pearlite transformation has been analyzed using a neural network technique within a Bayesian framework. An extensive database consisting of the detailed chemical composition considering elements such as Mn, Cr, Ni, Si and Mo, and isothermal temperature was compiled for this purpose using data from the published literature. With the aim of modeling the pearlite growth rate during the austenite-to-pearlite transformation a neural network has been proposed. The model allows us to examine the relative importance of the alloying elements in pearlite growth. The results from the network analysis were consistent with those expected from phase transformation theory.

1. Introduction

Pearlite is a lamellar structure of ferrite and cementite, which forms below the eutectoid temperature. The austenite transforms by a reconstructive mechanism, in which carbon and substitutional elements redistribute between ferrite and cementite. Pearlite nodules can nucleate on austenite grain boundaries, allotriomorphic ferrite grains or on cementite particles, depending upon steel composition. It is now generally agreed that during pearlite growth the alloying elements redistribute between the ferrite and cementite at low supersaturations (LE mechanism), and the growth is controlled by alloying element boundary diffusion. At higher supersaturations, pearlite growth occurs without any partitioning of the alloying element (NPLE mechanism) and it is controlled by carbon volume diffusion [1)]. The partitioning of alloying elements has been experimentally observed by Razik et al. [2)], Al-Salman et al. [3)], and Chance and Ridley [4)] in a number of Fe-C-Mn, Fe-C-Si, and Fe-C-Cr alloys. In all these studies, partitioning was detected at low supersaturations, whereas below a characteristic temperature of the steel, no-partition was found.

Most of the models reported in the literature deal with the theoretical calculation to determine the pearlite growth rate in steels such as Fe-C-X where X is the alloying element. This paper deals with analyzing the influence of alloying elements such as Mn, Cr, Ni, Si, and Mo, separately and together, on pearlite growth rate.

In this work a different approach is adopted involving the use of an artificial neural network to ‘blindly’ model a large set of published experimental data on pearlite growth rate in eutectoid steels. The results are then compared extensively against what might be expected on the basis of physical metallurgy theory.

2. Build of the model

2.1. The experimental database

To ideally model the pearlite growth rate, *G*, a complete description of the chemical composition and the isothermal transformation temperature is required. A search of the literature [-10)] allows us to collect 320 individual cases where detailed chemical composition, isothermal temperature, and growth rate values were reported. Table l shows the list of 6 input variables used for the pearlite growth rate analysis.

(Table I)

2.2. Brief description of neural network

An extensive description of neural network modeling was presented in the Part I of the present work. However, a brief summary of the method is described below as reminder.

The aim is to be able to estimate the pearlite growth rate as a function of the variables listed in Table I. In the present case, the network was trained using a randomly chosen of 160 examples from a total of 320 available; the remaining 160 examples were used as new experiments to test the trained network. Linear functions of the inputs x_j are operated by a hyperbolic tangent transfer function

$$h_i = \tanh\left(\sum_j w_{ij}^{(1)} x_j + \theta_i^{(1)} \right) \qquad (1)$$

so that each input contributes to every hidden unit. The bias is designated $\theta_i^{(1)}$ and is analogous to the constant that appears in linear regression. The strength of the transfer function is in each case determined by the weight $w_{ij}^{(1)}$. The transfer to the output y is linear

$$y = \sum_i w_i^{(2)} h_i + \theta^{(2)} \qquad (2)$$

This specification of the network structure, together with the set of weights, is a complete description of the formula relating the inputs to the output. The weights were determined by training the network and the details are described by MacKay [11-12]. The training involves a minimization of the regularized sum of squared errors. The term σ_v [13] used below was the framework estimation of the noise level of the data.

Figure 1 shows that the inferred noise level decreases monotonically as the number of hidden units increases in the model of pearlite growth rate. However, the complexity of the model also increases with the number of hidden units. A high degree of complexity may not be justified, and in an extreme case, the model may in a meaningless way attempt to fit the noise in the experimental data. MacKay [14] has made a detailed study of this problem and defined a quantity (the 'evidence') which comments on the probability of a model. In circumstances where two models give similar results for the known data, the more probable model would be predicted to be the simplest one; this simple model would have a higher value of evidence. The evidence framework was used to control σ_v. The number of hidden units was set by examining performance on test data. A combination of Bayesian and pragmatic statistical techniques were used to control the complexity of the model [-15]. Figure 1 also shows that a large number of hidden units did not give significantly lower values of σ_v; indeed, five hidden units were found to give a reasonable level of complexity to represent the variations of pearlite growth rate as a function of the input variables of Table I.

(Fig. 1)

However, it is possible that a *committee* of models can make a more reliable prediction than an individual model. The best models were ranked using the values of their test errors as Fig. 2(a) presents. Committee of models could then be formed by combining the prediction of the best *L* models, where L = l ,2,... Therefore, the size of the committee is given by the value of *L*.

The test error (T_{en}) [13] of the predictions made by a committee of *L* models, ranked 1 ,2...*q*...*L*, each with *n* lines of test data, is calculated in a similar manner to the test error of a single model [13]:

$$T_{en} = 0.5\sum_{n}\left(\overline{y_n} - t_n\right)^2$$
$$\overline{y}_n = \frac{1}{L}\sum_{q} y_n^{(q)} \qquad (3)$$

where $\overline{y}_n$ is the output of the committee, $y_n^{(q)}$ is the set of predictions made by the model, and t_n is the set of target (experimental) values.

The test error of the committee as a function of the models considered is plotted in Fig. 2(b). It is seen that the test error goes through a minimum for the committee made up of five models. Therefore, the neural network model used to calculate the pearlite growth rate in this paper is a committee of five models.

(Fig. 2)

From a comparison between Fig. 2(a) and Fig. 2(b) it is clear a reduction in test error and hence improved predictions by using the committee model approach instead of the best model alone. Comparison between the predicted and measured values of pearlite growth rate for the training and test data is shown in Fig. 3 for the best committee (consisting of five best models).

However, the practice of using a best-fit function does not adequately describe the uncertainties in regions of the input space where data are spare or noisy. MacKay [13-14)] has developed a particularly useful treatment of neural networks in a Bayesian framework, which allows us the calculation of error bars representing the uncertainty in the fitting parameters. The method recognizes that there are many functions which can be fitted or extrapolated into uncertain regions of the input space, without unduly compromising the fit in adjacent regions which are rich in accurate data. Instead of calculating a unique set of weights, a probability distribution of sets of weights is used to define the fitting uncertainty. The error bars therefore become larger when data are spare or locally noisy.

(Fig. 3)

Figure 4 illustrate the significance (σ_w) [13)] of each of the input variables, as perceived by the neural network, in influencing the pearlite growth rate. The metallurgical significance of the results predicted by the model is discussed below, but a first approximation of the influence of each one of the variables studied could be drawn from a close observation of Fig. 4. The transformation temperature clearly has a large intrinsic effect, which is consistent with experimental evidences reported in the literature over many decades. The content in manganese also has a strong effect on pearlite growth rate; the change on growth mechanism control from manganese diffusion at high temperatures (low supersaturation) to carbon

diffusion at low temperatures (high supersaturation) is dependent on manganese content and temperature as it was well established in literature. [2)] Chromium and molybdenum content in the steel also have a large effect on pearlite growth rate, as it was also established in literature. [1,16)] The influence of strong carbide forming elements on pearlite growth rate is two fold: first, the change from alloying element diffusion to carbon diffusion as the rate controlling mechanism, and second the solute drag effect on austenite→pearlite transformation front. On the other hand, the influence on pearlite growth rate of silicon is moderate, and nickel has the lowest effect on pearlite growth rate.

(Fig. 4)

3. Results and discussion

3.1. Pearlite growth rate in plain carbon steels

The goal of this paper is to model the growth rate of pearlite, and therefore to evaluate the influence of different alloy elements on the isothermal austenite-to-pearlite transformation. First of all, the neural network model was used to analyze the growth rate of pearlite in plain carbon steel. In this sense, Fig. 5 shows the evolution of the pearlite growth rate, *G*, with the isothermal temperature predicted by the model (solid line). The dashed lines represent the error bounds in calculations, *i.e.* the range of uncertainty on *G* predictions. Likewise, superimposed to the calculated trends the experimental data reported by Ridley and Brown [17)] are also presented in Fig. 5. It is clear that a good agreement between calculated and experimental results is obtained.

(Fig. 5)

3.2. Influence of alloying elements on pearlite growth rate

Figure 6 shows the neural network predictions for the evolution of pearlite growth rate with temperature for different steel grades. The influence of Mn and Ni decreasing the pearlite growth rate is clear from this figure. However, the effect of Cr, Mo, and Si on pearlite growth rate is not evident from Fig. 6 since the differences in pearlite growth rate between the different grades of Fe-C-X steels tested are due to the combination of the effect of alloying additions on Ae_1 temperature, and in the growth rate itself. In this sense, to isolate the effect of alloying elements on *G*, the evolution of pearlite growth as a function of undercooling ($\Delta T = T_E - T$) has been represented in Fig. 7. The comparison between graphs in Fig. 6 and Fig. 7 clearly illustrates this concern. For instance, the growth rate at 670 ºC varies from 12.5 to 0.3 μm s^{-1} when the Ni content is increased from 0.5 to 2.0 wt.-% (Fig. 6(c)). However, the temperature of 670 ºC corresponds to an undercooling of 44 ºC for a Fe-C-0.5Ni steel, meanwhile it corresponds to an undercooling of 20 ºC for a Fe-C-2.0Ni steel (Fig. 7(c)).

Figure 7 shows that all alloying elements decrease the pearlite growth rate. Moreover, it is shown that Mo yields the strongest decrease in the pearlite growth rate. Even a small amount of Mo such as 0.15 wt.-% reduces the growth rate by a factor of four relative to plain carbon steels, meanwhile the other strong-carbide former element, *i.e.* Cr, only modestly reduce the growth rate for a chromium content of 0.2 wt.-%. On the other hand, the results for Cr indicates that there are no significant differences between in growth rate when the alloy content is increased from 1 to 2 wt.-%.

Figure 8 compares the growth rate of pearlite in a Fe-C-X with the alloying element concentration for an undercooling of 50 ºC. The concentration in this graph has been

considered as X^*, which is the ratio between the X–element concentration ($[X]$) and the maximum concentration considered in at.-% ($[X]_{max}$, see Table I), *i.e.* $X^* = [X]/[X]_{max}$. One might conclude from this figure that Ni is the element with a minor effect on pearlite growth rate. By contrast, Si, Mn, Cr and Mo have a strong effect on pearlite growth rate. Such behavior from Cr and Mo is expected since both elements are very strong carbides formers and then are prone to solute drag effect, but it is interesting to note that Mn and Si affect pearlite growth in the same extent. Likewise, considering the concentration values tested, it is worth mentioning that Mo has the strongest effect decreasing pearlite growth rate. A molybdenum concentration of 0.4 in weight pct decreases in a hundred times the pearlite growth rate as compared with plain carbon steel for the same undercooling. These results are consistent with the well-established effect of molybdenum and chromium on isothermal transformation and hardenability.

(Fig. 6)

(Fig. 7)

(Fig. 8)

3.3. Analysis of pearlite growth rate in a Fe-C-X-Y steel

The ability to predict the evolution of pearlite growth rate in multicomponent steels is one of the main advantages of the model presented in this work against other models. In this sense, it has been compared the predictions of the model presented in this paper with the experimental values reported by Brown and Ridley [18] in a 0.61C-2.28Cr-2.02Ni-0.48Mo-0.28Mn-0.11Si

steel (Fig. 9). This figure shows the comparison between the predicted and experimental pearlite growth rate values. It could be concluded form this figure that there is an excellent agreement between predictions and measurements.

(Fig. 9)

It is observed in Fig. 9 a dramatic decrease in the pearlite growth rate as compared with plain carbon steel. This behavior has been attributed in the literature to solute drag effects which retard both nucleation and growth rates to similar extents. The mechanism of solute drag is uncertain but may be due to segregation of strong carbide forming element in carbon rich boundary regions ahead of the growing ferrite lamellae, where drastically carbon activity in austenite is reduced slowing down growth. [19] Nevertheless, other mechanism has been suggested by Sharma and Purdy: [20] the existence of clusters of strong carbides formers inhibits the growth of pearlite because of the necessity of carbon dissociate from the clusters before ferrite can grow.

An alternative explanation to this behavior might be suggested. The results presented in Fig. 9 could suggest that the growth of pearlite at very low temperatures is not a volume diffusion controlled reaction but rather an interface controlled process. The movement of an interface could be controlled both by diffusion of atoms, which provide the chemical concentration differences within each phase, and by a sluggish transfer of atoms across the interface, which does not give rise to any large concentration differences. The former is referred to as volume diffusion-controlled process, and the latter as an interface-controlled. [21]

The rate of reaction controlled by interface process is given by the following equation: [22]

$$G_I = \delta\nu \exp\left(-\frac{\Delta Q}{RT}\right)\left[1-\exp\left(-\frac{\Delta G^{\beta\alpha}}{RT}\right)\right] \tag{4}$$

where δ is the width of the interface, R is the ideal gas constant, T is the absolute temperature, ΔQ and $\Delta G^{\beta\alpha}$ are the activation energy and the driving force for the transformation per atom, and ν is a characteristic frequency which is given by kT/h where k and h are Boltzmann's and Plank's constants respectively.

The value of $\Delta G^{\beta\alpha}$ is calculated as the free energy change due to the formation of pearlite from austenite as follows: [23)]

$$\begin{aligned}\Delta G^{\beta\alpha} = &\left(1-x^{\gamma}\right)\Delta G_{Fe}^{\gamma\to\alpha} + x^{\gamma}\left(\Delta G^{\theta} + 4.01T - 10580\right) \\ &- RT\left[\frac{1-x^{\gamma}}{5}\ln\left(\frac{1-6x^{\gamma}}{1-x^{\gamma}}\right) + x^{\gamma}\ln\left(\frac{x^{\gamma}}{1-6x^{\gamma}}\right)\right]\end{aligned} \tag{5}$$

where x^{γ} is the carbon concentration in austenite, and

$$\begin{aligned}\Delta G_{Fe}^{\gamma\to\alpha} &= -7115.8 + 9.542T - 2.833\times10^{-3}T^2 \\ \Delta G^{\theta} &= 27602.08 - 25.828T\end{aligned} \tag{6}$$

Both expressions in J mol^{-1}. Assuming that δ being the lattice parameter of austenite, ν being kT/h = 1.57×10^{13} s^{-1}, the growth rate controlled by interface process can be calculated using equation (4) as a function of the activation energy ΔQ. Since the growth rate of pearlite at 570 ºC of 0.61C-2.28Cr-2.02Ni-0.48Mo-0.28Mn-0.11Si steel was measured to be 1.25×10^{-9} m s^{-1} by Brown and Ridley [18)], the activation energy ΔQ can be calculated from the equation (4).

Values of ΔG^{θ} and $\Delta G_{Fe}^{\gamma\to\alpha}$ are 5829 and –1086 J mol^{-1}, hence $\Delta G^{\beta\alpha}$ = –1721 J mol^{-1}, respectively. Using the data $\delta = 3.573\times10^{-10}$ m and $\nu = 1.57\times10^{13}$ s^{-1}, ΔQ is calculated to be 194 kJ mol^{-1}, which is close to the activation energies of the self diffusion of iron in austenite and ferrite, *i.e.* 286 and 240 kJ mol^{-1}, respectively. Although the activation energy calculated from the observed growth rate at 570 ºC is close to that for self-diffusion of iron, it is still uncertain if reaction is controlled by the interface process. Further work is necessary.

3.4. Growth mechanism control

The growth rate of pearlite is believed to be controlled by either volume diffusion of carbon [24-25] or by grain boundary diffusion of substitutional alloying element. [6,26] The two theories are summarized as follows.

When the growth rate of pearlite is controlled by the bulk diffusion of atoms in austenite ahead the interface, the diffusion of carbon may play a more important role than that of substitutional alloying elements, since the diffusivity of the substitutional alloying elements may not diffuse a long distance during the reaction. The growth rate of pearlite (G_C) is expressed as follows: [6]

$$G_C = \frac{D_C^{\gamma}\left(x_1^{\gamma\alpha} - x_1^{\gamma\theta}\right)}{g\left(x_1^{\theta\gamma} - x_1^{\alpha\gamma}\right)}\frac{S_o}{S_\alpha S_\theta}\left[1-\frac{S_c}{S_o}\right] \qquad (7)$$

where g is a geometric factor equal to 0.72; D_C^{γ} is the carbon diffusion coefficient in austenite; $x_1^{\gamma\alpha}$ is the carbon concentration at the austenite–ferrite interface in austenite; $x_1^{\gamma\theta}$ is the carbon concentration at the austenite–cementite interface in austenite; $x_1^{\alpha\gamma}$ is the carbon

concentration at the austenite–ferrite interface in ferrite; $x_1^{\theta\gamma}$ is the carbon concentration at the austenite–cementite interface in cementite; S_c is the theoretical critical spacing at which the growth rate becomes zero; S_θ and S_α are the thickness of cementite and ferrite lamellae, respectively. The ratio between S_θ and S_α was assumed to be 7.

When the partitioning of the substitutional alloying elements is substantial during the growth event of pearlite, boundary diffusion of the alloying elements may control the growth rate of pearlite, since the boundary diffusivity of the substitutional alloying elements may become comparable to the bulk diffusivity of carbon in austenite, and, as a result, a long range diffusion of the substitutional alloying elements may become possible during the reaction. The growth rate in the case (G_X) is expressed as follows: [19)]

$$G_X = 12KD_B^\gamma \delta \frac{\left(x_2^{\gamma\alpha} - x_2^{\gamma\theta}\right)}{\bar{x}_2} \frac{1}{S_\alpha S_\theta}\left[1 - \frac{S_c}{S_o}\right] \tag{8}$$

where K is the boundary segregation coefficient which is the ratio between alloying element concentration in austenite near the boundary and that in the boundary; D_B^γ is the boundary diffusion coefficient of substitutional alloying element; δ is the thickness of the boundary; $x_2^{\gamma\alpha}$ is the substitutional alloying element concentration at the austenite–ferrite interface in austenite, $x_2^{\gamma\theta}$ is the substitutional alloying element concentration at the austenite–cementite interface in austenite; and $\bar{x}_2$ is the average substitutional alloying element concentration in the alloy concerned.

Equations (7) and (8) give the relationship between growth velocity, spacing, concentration gradient and diffusivity. Since the concentration gradient term is approximately proportional to undercooling, and undercooling is proportional to reciprocal spacing, $1/S_o$, (eq. (6) and (7)

in Part I paper of this work) for volume diffusion control growth the equation (7) may be rewritten as:

$$G_C S_o^2 = k_1 D_C^\gamma \tag{9}$$

while for boundary diffusion control equation (8) may be rearranged to give

$$G_X S_o^3 = k_2 D_B^\gamma \tag{10}$$

where k_1 and k_2 are constants. Hence, logarithmic plots of $G_C \big/ D_C^\gamma$ or $G_X \big/ D_B^\gamma$ versus $1 / S_o$ should give straight lines with slopes of 2 or 3, depending on whether growth is controlled by volume or boundary diffusion.

As reported by Fridberg *et al* [27], the boundary diffusivities of the closest neighbors of iron in the periodic system, such as Cr, Mn, Ni, and Mo, are the same as the self-boundary diffusion coefficient of iron in austenite. Thus, $D_B^\gamma \delta$ in eq. (8) can be expressed as 5.4×10^{-14} exp (-155500 / *RT*) in $m^3\ s^{-1}$ where δ is the grain boundary thickness (reasonable value of 2.5×10^{-10} m). [22] Regarding Si, there is lack of boundary diffusivities data in literature. Therefore, since it is well known that boundary diffusion is much more faster than bulk diffusion, it is a sensible approximation to consider the activation energy as the half of that for silicon self-diffusion. [28] In this case, D_B^γ could be considered as 0.03×10^{-4} exp(-101000 / *RT*) in $m^2\ s^{-1}$.

On the other hand, calculations of D_C^γ have been carried out according to Bhadeshia. [29] The author considers both the kinetic and equilibrium thermodynamic behavior of carbon in austenite. These calculations also takes into account the concentration dependence of the

activity of carbon in austenite, and the repulsive interactions between the nearest neighboring carbon atoms located in octahedral interstitial sites. Thus, D_C^{γ} is calculated by two factors: one of them is a concentration dependent factor and the other one is independent,

$$D_C^{\gamma} = \xi(\theta)\frac{k_B T}{h}\left(\frac{\lambda^2}{3\gamma_m}\right)\exp\left\{-\frac{\Delta G^*}{k_B T}\right\} \qquad (11)$$

where $\xi(\theta)$ is the carbon concentration dependent factor obtained according to Bhadeshia's calculations 29); ΔG^* is the activation energy for diffusion; γ_m is an activity coefficient assumed constant; λ is the distance between the {002} austenite planes and h is the Planck's constant. Bhadeshia 29) found that $\Delta G^* / k_B$ = 21230 K and ln (γ_m / λ^2) = 31.84.

(Fig. 10)

Figure 10 shows the logarithmic plots of $G_C \big/ D_C^{\gamma}$ against $1 / S_o$ for a plain carbon steel. Likewise, Figs. 11 and 12 show the logarithmic plots of $G_C \big/ D_C^{\gamma}$ and $G_X \big/ D_B^{\gamma}$ versus $1 / S_o$ for each one of the alloying elements considered, respectively. The values of the interlamellar spacing were calculated according to the Part I paper of this work.

Data presented in Fig. 10 fall clearly in a straight line with a slope m=2. Therefore, it is clear that volume diffusion of carbon in austenite is the dominant process controlling pearlite growth in pure Fe-C steels.

(Fig. 11)

(Fig. 12)

From the results presented in Figs. 11 and 12 some conclusions can be drawn. Some authors have reported [2)] that Mn partitions preferentially into the pearlitic cementite at the transformation interface above a certain temperature (no-partition temperature) which depends on manganese concentration of the steel, *i.e.* manganese partitions into pearlitic cementite at high reaction temperatures, but not at lower temperatures. Above the no-partition temperature manganese diffusion is rate controlling and below this temperature carbon diffusion controls the rate of pearlite growth. These results are consistent with the analysis from the data presented in Fig. 11(a) and 12(a). It is clear that the data fitted well to a straight line of slope m=2 at low temperatures (high values of Log $(1 / S_o)$) for increasing manganese content (Fig. 11(a)), meanwhile the data are fairly good adjusted to a straight line of slope m=3 in Fig. 12(a) at high temperatures (low values of Log $(1 / S_o)$) for increasing manganese content. However, the results are no clear for a manganese concentration of Mn=0.25 wt.-% since the data fall with the same level of accuracy to a straight line of slopes m equal 2 (Fig. 11(a)) or 3 (Fig. 12(a)), which might indicate that both growth control mechanisms act simultaneously.

Figure 13 shows the evolution of the ratio between the growth rate calculated for two very different degree of undercooling, i.e. an undercooling of 120 ºC and 20 ºC, with manganese content. This figure indicates a change in the rate controlling mechanism as Mn content increases. As it is shown in the figure, as Mn increases, the ratio increases, which indicates that growth rate at high undercooling is faster than at low undercoolings. It could be concluded that a change in rate controlling process is produced and it is likely that the rate of pearlite is carbon diffusion rate controlling at high undercooling, since boundary diffusion is a sluggish mechanism as compared with volume diffusion of carbon.

(Fig. 13)

Figures 11(c) and 12(c) show that data predicted by the neural network model for a Fe-C-Ni steel fall perfectly over a straight line of slope m=2. Hence, the growth control in pearlite of steels containing additions of Ni is by carbon diffusion at all temperatures. The effect of Ni in decreasing the rate of pearlite growth is primarily due to constitutional effects *i.e.* to its effect on the Ae_1 temperature. Carbon diffusion is rate controlling and the partitioning of Ni observed experimentally has gone together with the rate controlling process (carbon diffusion). [17)]

Results for Si are in full agreement with predictions reported by Hillert [8)]. This author proposed that for most of the examined temperatures range, the rate of formation of pearlite is controlled by interfacial diffusion of silicon, since the data presented in Fig. 12(d) follow a straight line with slope m=3. Maybe, this behavior is caused by the growth of pearlite in a silicon steel depends more critically upon lowering of the silicon content in the cementite than the increase in the ferrite. This is because cementite cannot grow with too much silicon. [30-32)] In order to satisfy this practical requirement it is sufficient to diffuse silicon over distances comparable with the thickness of the cementite lamellae rather than the ferrite lamellae which are about seven times large. This might be the reason why the effect of silicon on hardenability is not as substantial as partitioning of substitutional elements would normally lead to.

It has been reported in the literature that both Cr and Mo partition at the pearlite reaction front over a wide range of temperatures. [4,16)] Hence, for chromium steels at higher reaction temperatures calculations which assume interfacial diffusion of chromium to be rate controlling give good agreement (Fig. 12(b) for low values of Log $(1 / S_o)$), as was previously

reported by Chance and Ridley. [4] By contrast, the predicted pearlite growth rates agree fairly well with the assumption of carbon diffusion as rate controlling at low temperatures (high values of Log $(1 / S_o)$ in Fig. 11(b)). However, Chance and Ridley argued that this agreement may be fortuitous, and it is likely that the divergence is attributed to 'solute drag' which retards interface movement. The solute drag effect is associated with the development of an austenite bay in the isothermal transformation curve which pushes the pearlite nose to higher temperatures. This assumption might explain the situation presented in Figs. 6 and 7 where it seems that growth rates are concentration dependent at lower temperatures.

A similar behavior is observed for the other strong carbide former element studied, *i.e.* molybdenum. It could be concluded from the results presented in this work that at higher reaction temperatures molybdenum diffusion seems to be the rate controlling process in Fe-C-Mo steels (low values of Log $(1 / S_o)$ in Fig. 12(e)). However, no conclusive results are obtained for low temperatures (high values of Log $(1 / S_o)$ in Fig. 11(e)) where the results seems to fall on a straight line of slope m=2, and hence carbon diffusion could be the rate controlling mechanism. The divergence in the results presented for low temperatures in Fig. 12(e) (high values of Log $(1 / S_o)$) could be attributed again to 'solute drag' effects.

4. Conclusions

1. A neural network method based on a Bayesian framework has been used to rationalize the published experimental data on pearlite growth rate of steels. Neural networks are clearly useful in recognizing pattern in complex data. The resulting quantitative models are transparent; they can be interrogated to reveal patterns and the model parameters can be studied to illuminate the significance of particular variables. A trained network embodies the knowledge within the training dataset, and can be adapted as knowledge is accumulated. It is now possible, therefore, to estimate the role of elements such as Mn, Cr,

Ni, Si and Mo which are traditionally used as alloying elements in steel industry. The results of this work demonstrate that an increase of Mn, Cr, Ni, Si and Mo content drops the velocity at which pearlite grows.

2. It has been shown that boundary diffusion at high temperatures and volume diffusion at low temperatures are the respective growth mechanism control in a Fe-C-Mn steel. Likewise, it could be concluded that an increase in manganese content dramatically decreases pearlite growth rate.
3. The influence of nickel on pearlite transformation in a Fe-C-Ni steel is not as dramatic as chromium and manganese. The effect of Ni in decreasing the rate of pearlite growth is due primarily to constitutional effects *i.e.* to its effect on the Ae_1 temperature. Carbon diffusion is rate controlling.
4. Silicon diffusion is the rate controlling mechanism in Fe-C-Si steels. This is consistent with the partition of silicon to pearlitic ferrite reported in literature 3) for a wide range of temperatures but diffusion is rapid and the diffusion path is short so that the retardation of pearlite growth is not appreciable.
5. Interfacial diffusion of the strong carbide formers elements such as Cr and Mo partition at the whole pearlite formation temperature range is the rate controlling mechanism in Fe-C-Cr and Fe-C-Mo steels, respectively. The growth rate is markedly retard by the necessity for molybdenum and chromium to partition which is consistent with the well-established effect of both elements on isothermal transformation and hardenability of Fe-C-Mo and Fe-C-Cr steels. On the other hand, carbon diffusion could be the rate controlling mechanism at low temperatures, although the existence of solute drag effects make difficult to obtain some conclusions to this respect.

Acknowledgements

The authors acknowledge financial support from Spanish Ministerio de Ciencia y Tecnología (MAT2001-1617). C. Capdevila would like to express his gratitude to the Consejo Superior de Investigaciones Cientifícas for financial support as a Post-Doctoral contract (I3P PC-2001-1). F.G. Caballero would like to thank the Spanish Ministerio de Ciencia y Tecnología for the financial support in the form of a Ramon y Cajal contract. The authors are also grateful to Neuromat Ltd. for the provision of the neural network software used in this work.

References

1) R. C. Sharma, G. R. Purdy and J. S. Kirkaldy: Metall Trans. A, **10A** (1979), 1129.

2) N. A. Razik, G. W. Lorimer and N. Ridley: Acta Metall., **22** (1974), 1249.

3) S. A. Al-Salman, G. W. Lorimer and N. Ridley: Acta Metall., **27** (1979), 1391.

4) J. Chance and N. Ridley: Metall. Trans., **12A** (1981), 1205.

5) M.P. Puls and J. S. Kirkaldy: Metall. Trans., **3** (1972), 2777.

6) B.E. Sundquist: Acta Metall., **17** (1969), 967.

7) K. Hashiguchi and J. S. Kirkaldy: Scan. J. Metall., **13** (1984), 240.

8) M. Hillert: Proc. of Int. Conf. in Solid-Solid Phase Transformations, ed. by H.I. Aaronson, D. E. Laughlin, R. F. Sekerka, C. M. Wayman, TMS-AIMME, Warrendale, (1980), 789.

9) M. L. Picklesimer, D. L. McElroy, T. M. Kegley, E. E. Stansbury and J. H. Frye: Trans. Am. Inst. Min. Metall. Eng. (A.I.M.M.E), **218** (1960), 473.

10) J. H. Frye, E. E. Stansbury and D. L. McElroy: Trans. Am. Inst. Min. Metall. Eng. (A.I.M.M.E), **197** (1953), 219.

11) D. J. C. MaKay: Neural Comput., **4** (1992), 698.

12) D. J. C. MaKay: Darwin college J., **March** (1993), 81.

13) D. J. C. MaKay: Neural Comput., **4** (1992), 415.

14) D. J. C. MaKay: Neural Comput., **4** (1992), 448.

15) H. K. D. H. Bhadeshia: ISIJ Int., **39** (1999), 965.

16) N. Ridley: Proc of an Int. Conf. in Ferrous Alloys, ed. by A. R. Marder and J. I. Goldsteian, TMS-AIMME, Warrendale, (1984), 201.

17) D. Brown and N. Ridley: J. Iron Steel Inst, **207** (1966), 1232.

18) D. Brown and N. Ridley: J. Iron Steel Inst, **204** (1966), 811.

19) M. Hillert: The mechanism of phase transformations in crystalline solids, Institute of Metals, London, (1969), 231.

20) R. C. Sharma and G. R. Purdy: Metall. Trans., **4** (1973), 2302.

21) M. Hillert: Metall. Trans. A, **6A** (1975), 5.

22) J. W. Christian: Theory of transformations in Metals and Alloys – Part I, 3rd edition, Pergamon Press, Oxford, (2002), 480.

23) L. Kaufman and S. V. Radcliffe: Decomposition of Austenite by Diffusional Process, ed. by V. F. Zackay and H. I. Aaronson, Interscience Publishers, New York, (1962), 313.

24) C. Zener: Trans. Am. Inst. Min. Metall. Eng. (A.I.M.M.E), **167** (1946), 550.

25) M. Hillert: Jerkont. Ann., **141** (1957), 757.

26) J. M. Shapio and J. S. Kirkaldy: Acta Metall., **16** (1968), 579.

27) J. Fridberg, L. -E Törndahl, and M. Hillert: Jernkont. Ann., **153** (1969), 263.

28) D. A. Porter and K.E. Easterling: Phase Trasnformation in Metals and Alloys, 2nd edition, Chapman & Hall, London, (1992), 98.

29) H. K. D. H. Bhadeshia: Metal Sci., **15** (1981), 477.

30) F. G. Caballero, H. K. D. H. Bhadeshia, K. J. A. Mawella, D. G. Jones and P. Brown: Mater. Sci. Technol., **17** (2001), 512.

31) F. G. Caballero, H. K. D. H. Bhadeshia, K. J. A. Mawella, D. G. Jones and P. Brown: Mater. Sci. Technol., **17** (2001), 517.

32) F. G. Caballero, H. K. D. H. Bhadeshia, K. J. A. Mawella, D. G. Jones and P. Brown: Mater. Sci. Technol., **18** (2002), 279.

Table I. Variables that influence Pearlite Growth Rate. SD is standard deviation

		Minimum	Maximum		Average	SD
		wt.-%	wt.-%	at.-%		
Inputs	Mn	0.00	1.80	1.77	0.4204	0.64100
	Cr	0.00	3.28	3.41	1.8675	0.5213
	Ni	0.00	3.00	2.77	1.0089	0.6044
	Si	0.00	2.50	4.71	0.2538	0.6314
	Mo	0.00	0.50	0.28	0.4801	0.2456
	T, ºC	570.00	752.00		660.0000	40.3861
Output	LogG, μm/s	-2.15	1.79		0.3690	0.8249

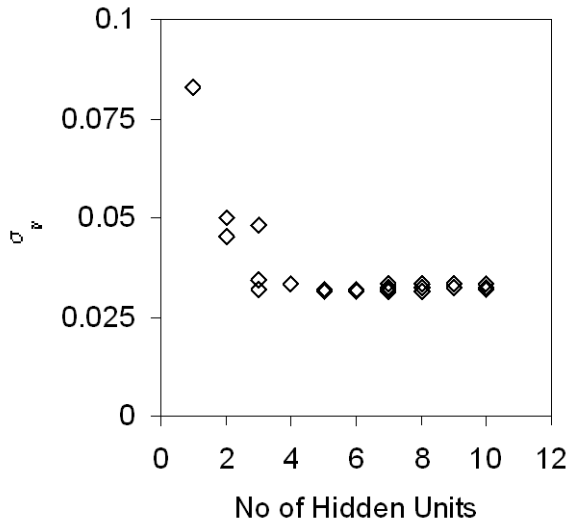

Figure 1. Variation of inferred noise level (σ_V) as a function of the number of hidden units.

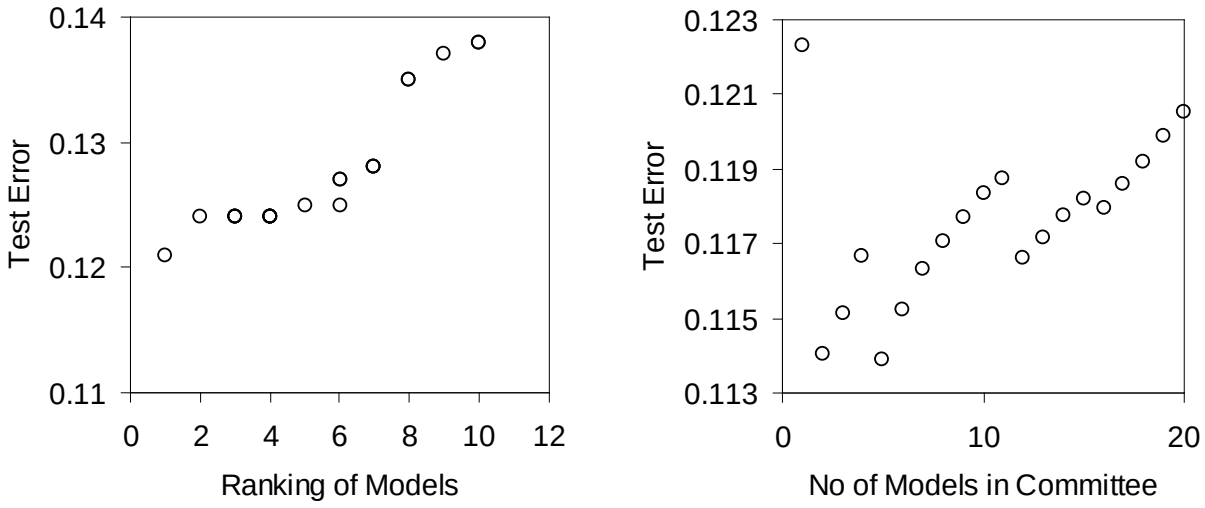

(a) (b)

Figure 2. Test error values of (a) the twelve best pearlite growth rate models, and (b) the committee.

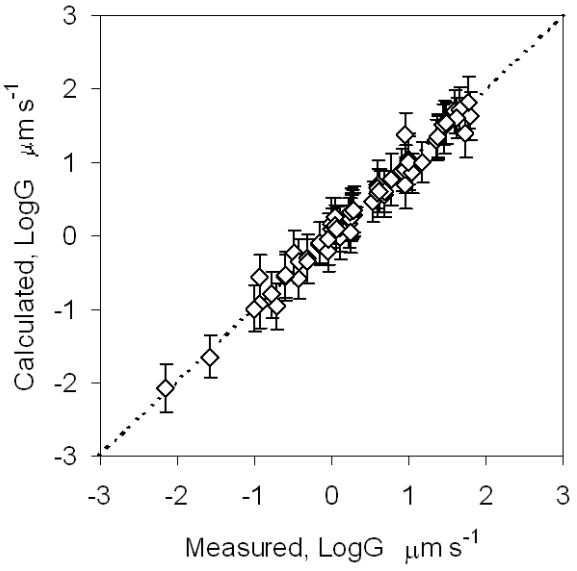

Figure 3. Comparison between the predicted and measured values of pearlite growth rate using the five models committee.

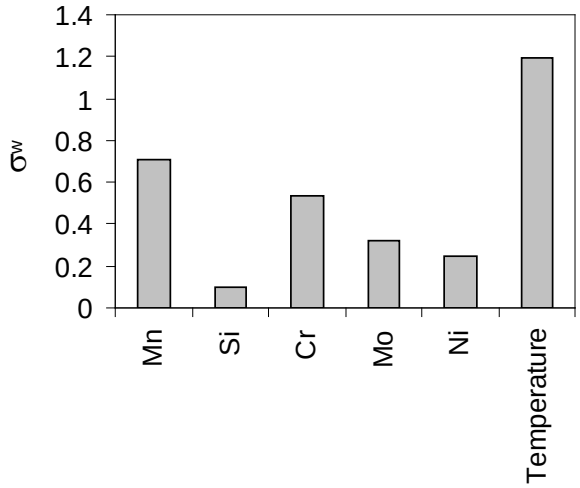

Figure 4. Histogram showing the significance of input variables in influencing pearlite growth rate perceived by the model.

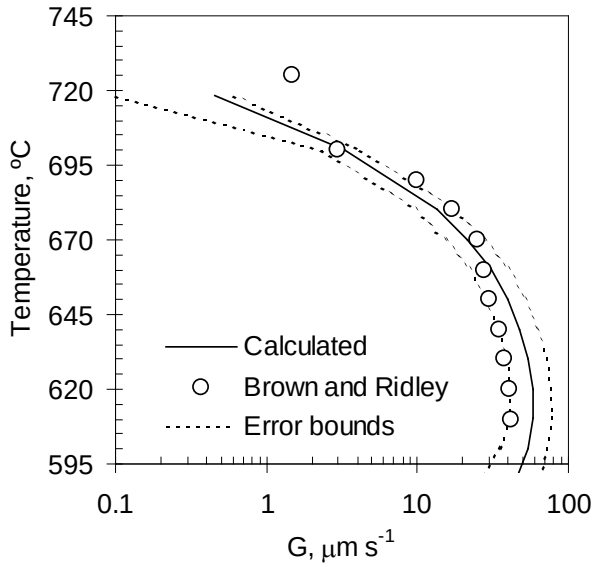

Figure 5. Evolution of pearlite growth rate in Fe-C steels.

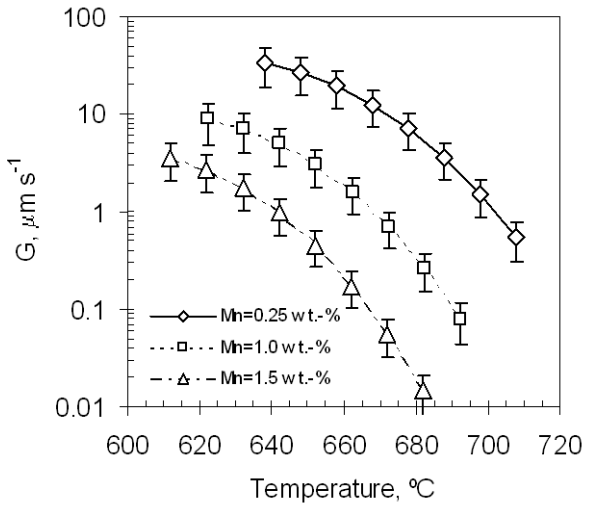

(a)

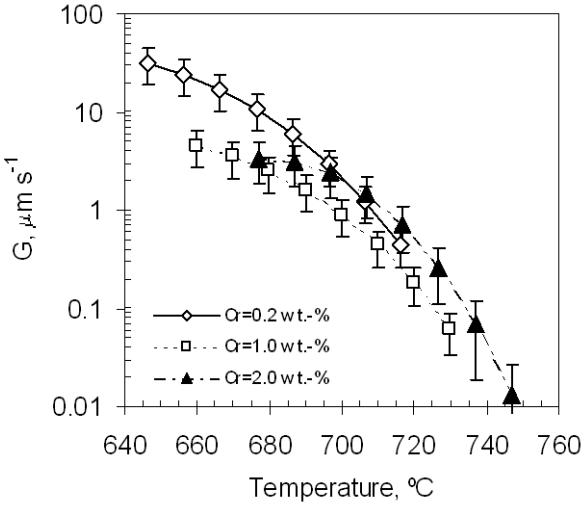

(b)

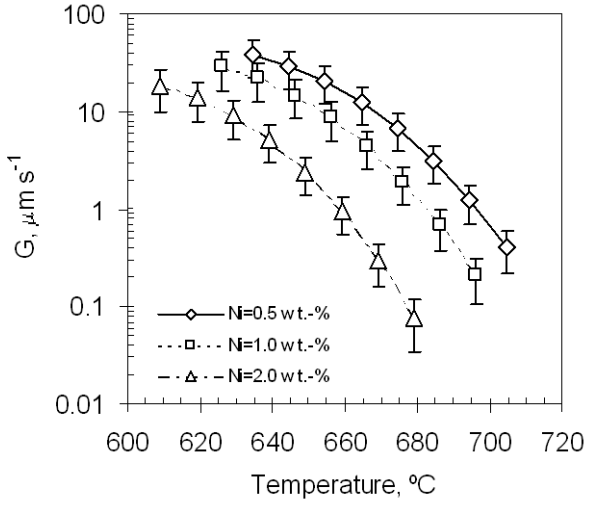

(c)

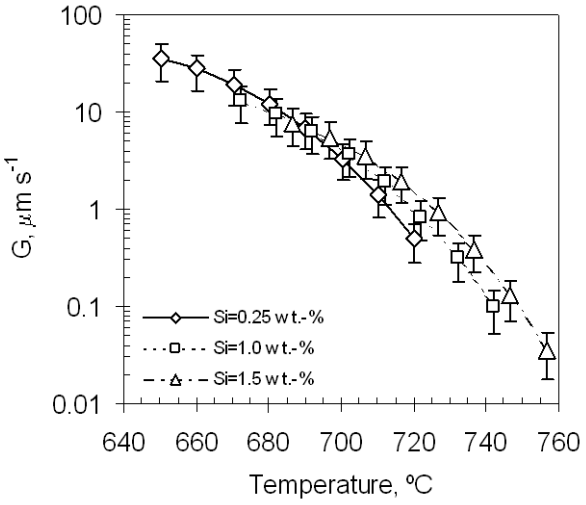

(d)

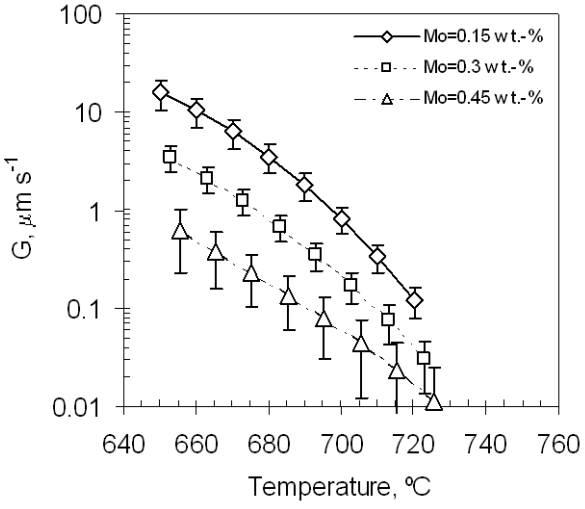

(e)

Figure 6. Predicted pearlite growth rate as a function of temperature for different grades of (a) Mn, (b) Cr, (c) Ni, (d) Si, and (e) Mo.

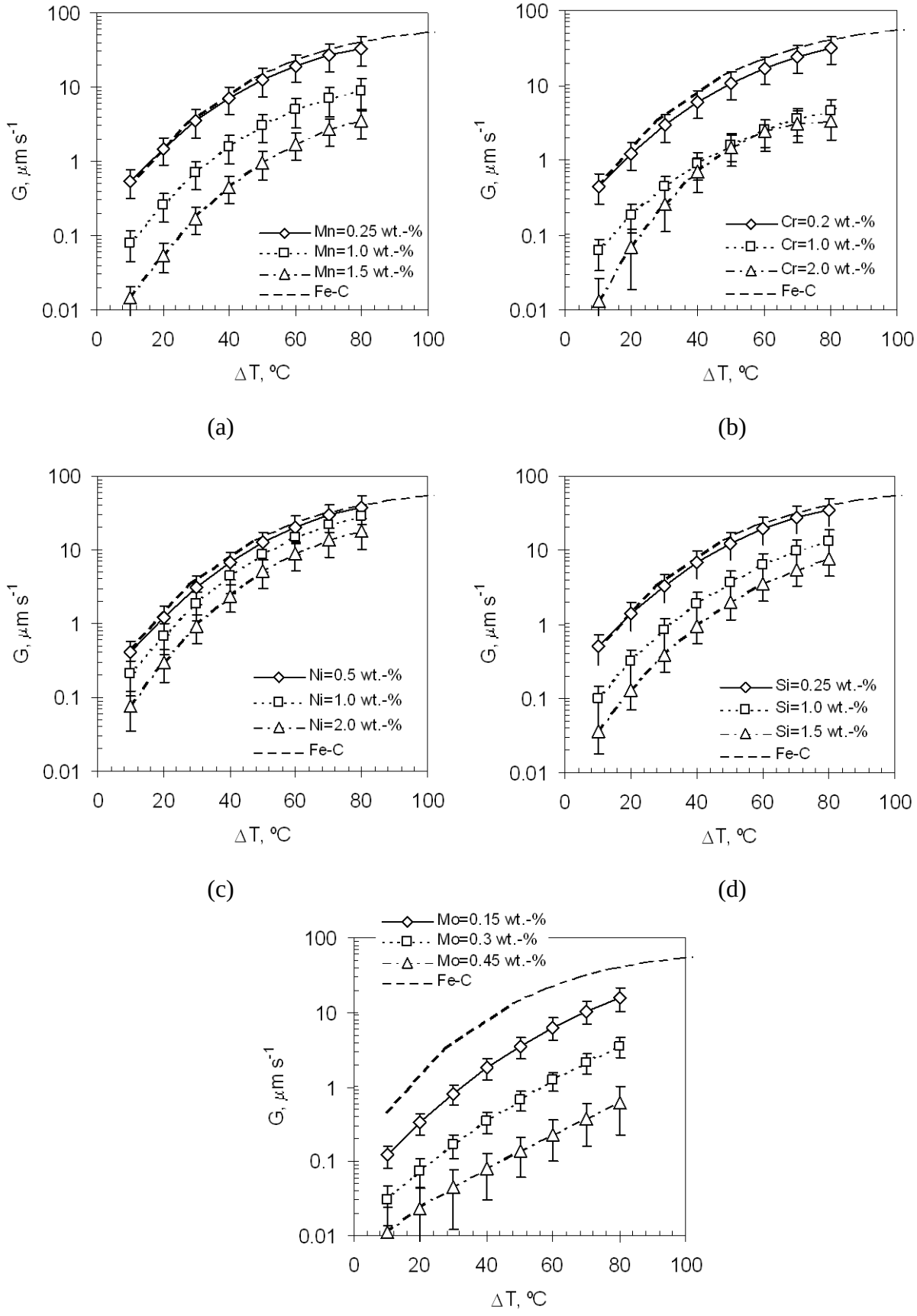

Figure 7. Pearlite growth rate vs. undercooling for different grades of (a) Mn, (b) Cr, (c) Ni, (d) Si, and (e) Mo.

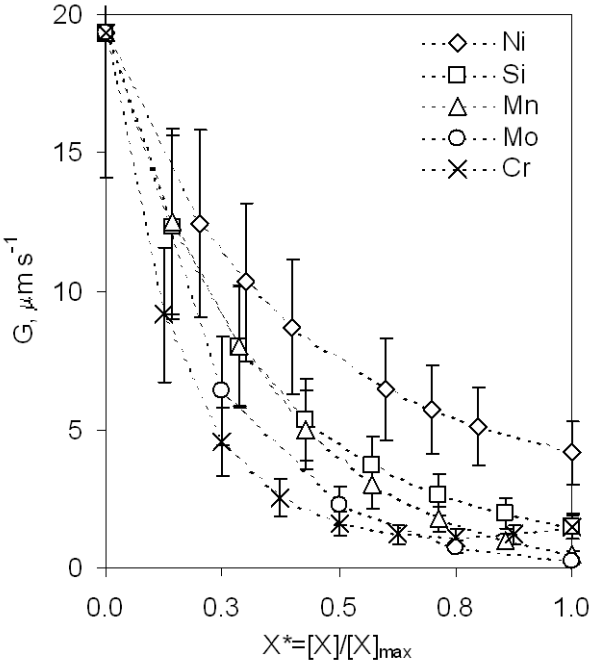

Figure 8. Effect of Mn, Cr, Ni, Si and Mo on pearlite growth rate for a fixed undercooling of 50 ºC

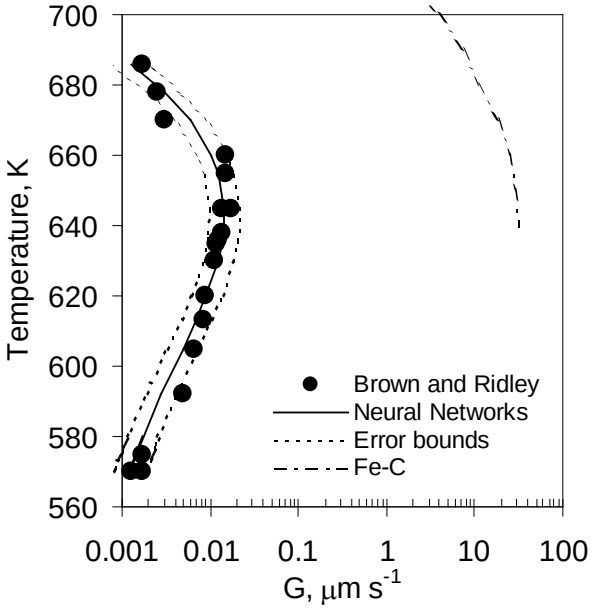

Figure 9. Evolution of pearlite growth rate in a Fe-C-Mn-Cr-Ni-Si-Mo steel

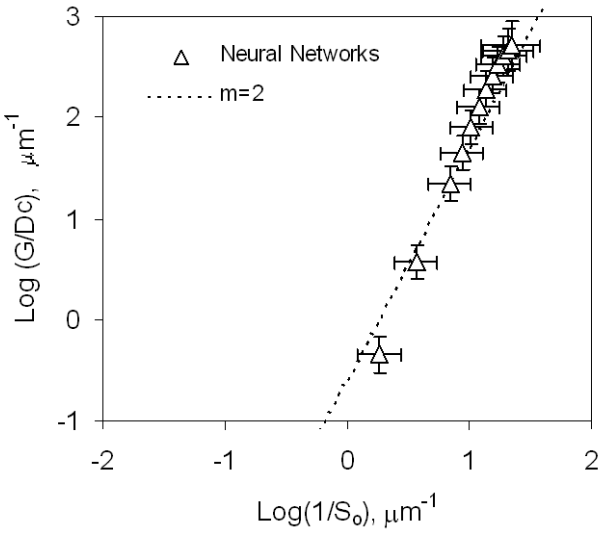

Figure 10. Spacing-velocity relationship for plain carbon steels.

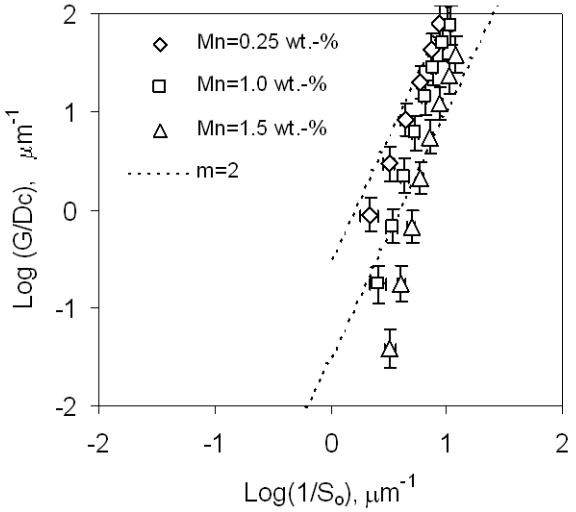

(a)

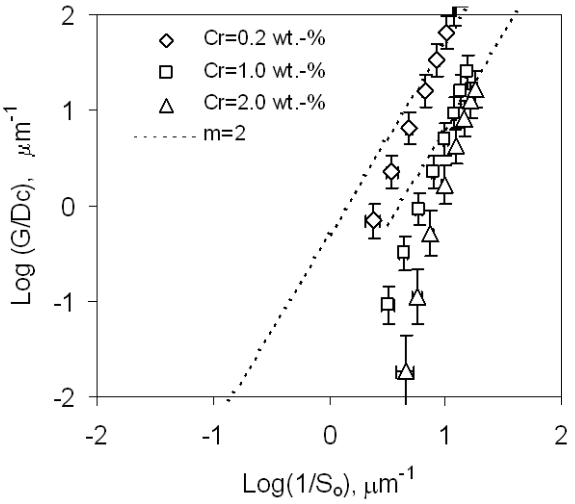

(b)

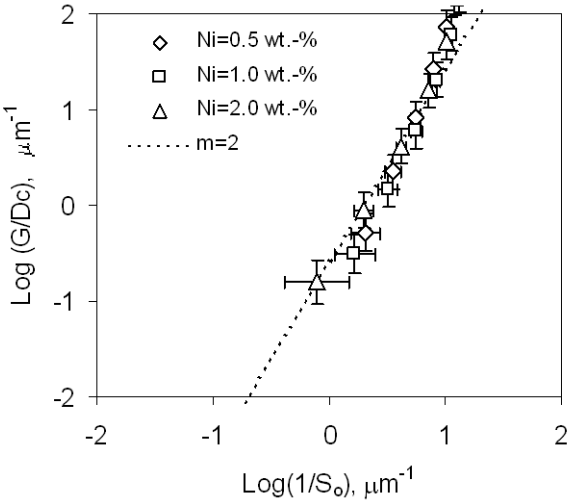

(c)

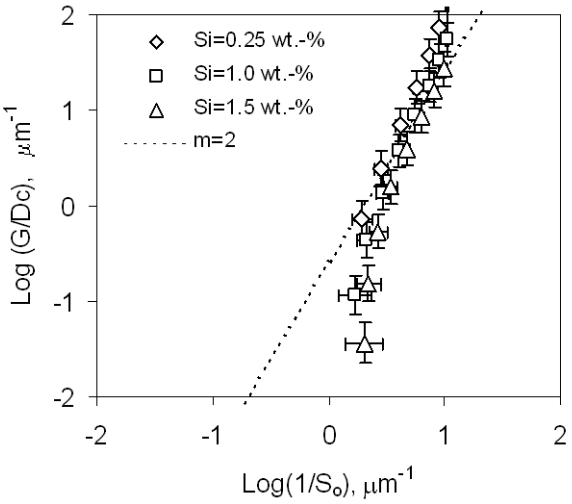

(d)

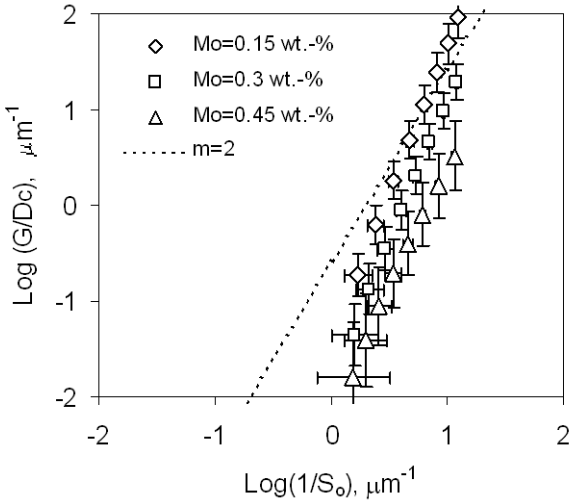

(e)

Figure 11. Log($G_C \big/ D_C^{\gamma}$) vs Log ($1 / S_o$) plots for (a)Mn, (b)Cr, (c)Ni, (d)Si, and (e)Mo eutectoid steels.

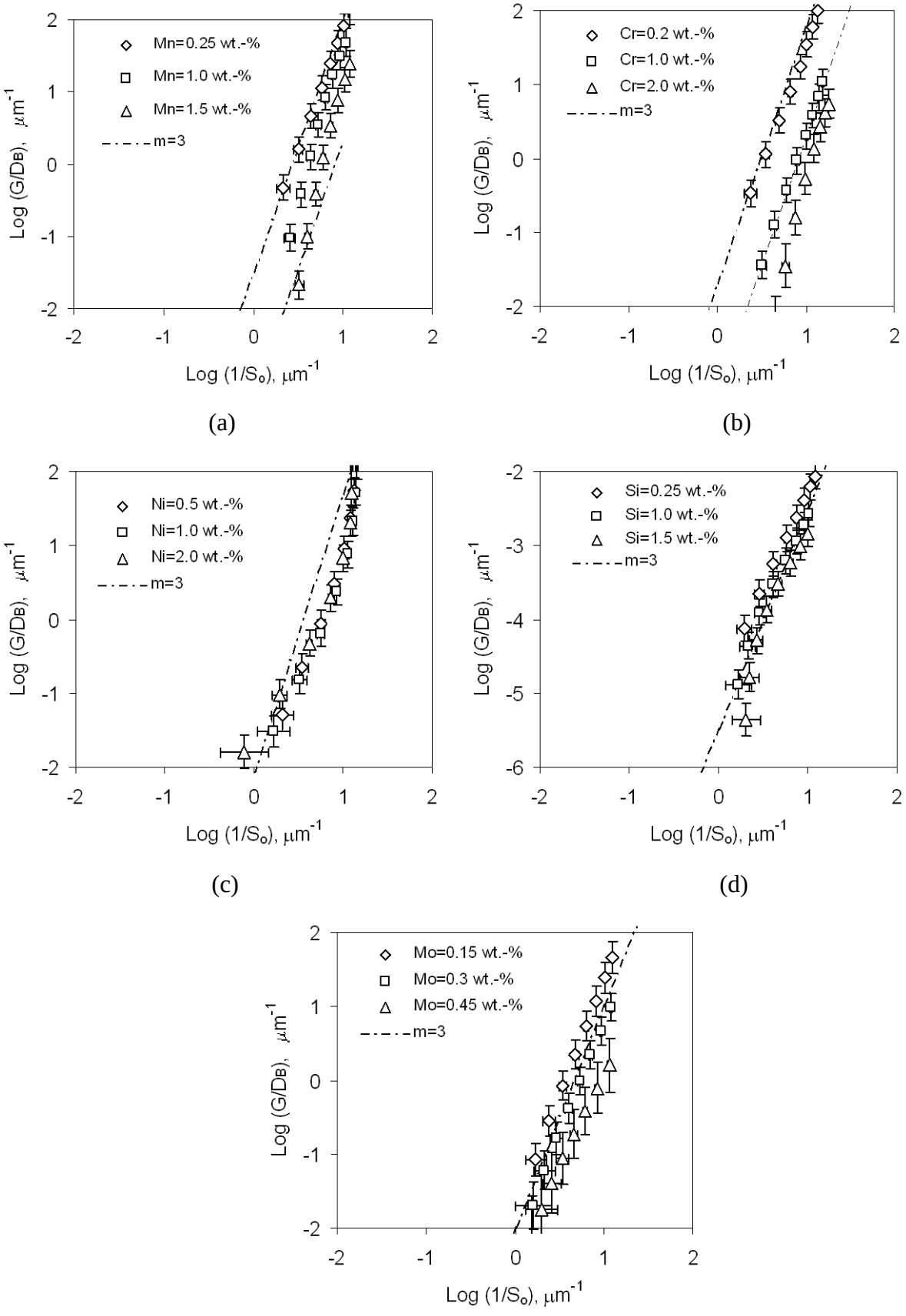

Figure 12. Log(G_X / D_B^{γ}) vs Log ($1 / S_o$) plots for (a)Mn, (b)Cr, (c)Ni, (d)Si, and (e)Mo eutectoid steels.

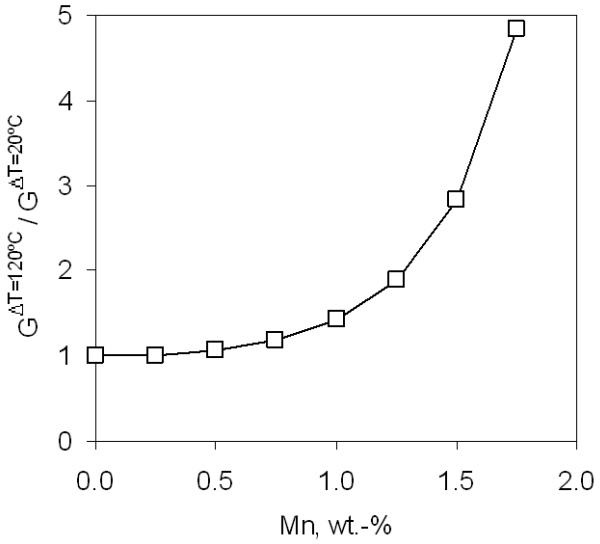

Figure 13. Ratio between growth rates for 120 ºC and 20 ºC of undercooling.